TRACKING PERFORMANCES OF THE DIMUON SPECTROMETER WITH A DIPOLE MAGNET

J.P. Cussonneau, H. Gutbrod, P. Lautridou, L. Luquin, V. Métivier, V. Ramillien

Laboratoire SUBATECH, UMR Université, Ecoles des Mines, IN2P3/CNRS, F-44070 Nantes Cedex 03, France

Abstract

The tracking performances of the ALICE forward muon spectrometer, with a dipole magnet, are investigated in this note. The study concerns the track finding and the mass resolution as well as the acceptance of the spectrometer for the Φ 's, J/Ψ 's and Υ 's. With the proposed setup, a mass resolution below 100 MeV is obtained and a track finding efficiency better than 90 % is achieved for the heavy resonance. An absolute acceptance of 4.83 % is found which is acceptable in order to reach the requiered statistic for Υ' and Υ'' in Pb-Pb collisions.

Contents

1 Tracking Overview

The general lay-out of the setup and its integration with the central detector is shown on figure 1. Compared to the LOI magnet [1] [2], the opening of the dipole has been reduced to 9° and the front of the dipole is moved behind the L3 door at 7.25 m from the vertex. The two tracking planes, used for the sagitta measurements inside the LOI dipole have been jointed side by side in the middle of the magnet in order to have the same characteristics than the four outside tracking stations. Apart from that, the material compositions (absorber, beam shielding, tracking chambers, etc..) are kept identical to the LOI ones [3].

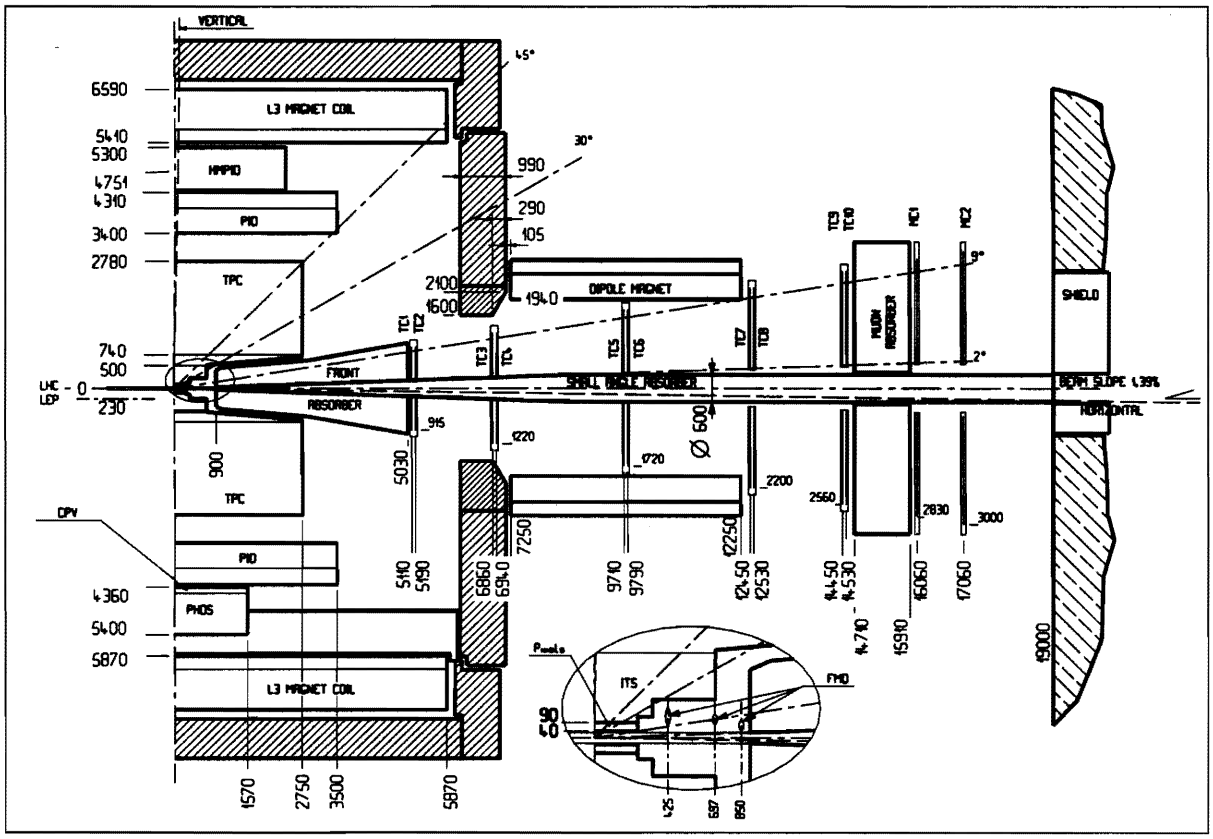

Figure 1: *Lay-out of the 9° dipole spectrometer and its integration in ALICE as used for the GEANT simulations.*

To estimate the tracking performances of the dimuon spectrometer, a chain of simulation and reconstruction programs has been developped. Calculations are based on the GEANT package for the set-up description and FORTRAN codes for the event generators and reconstruction procedures. All relevant physics processes are included in the simulation (e.g. multiple scattering, energy loss, bremsstrahlung, etc.). The following parameters are fixed for all tracking simulations:

- Because when using muons the displacement due to absorber multiple scattering is larger than the position resolution given by the ITS [4], the vertex resolution is not

taken into account. The diamond point is fixed at (0,0,0) for the particle emissions.

- An homogenous square shaped magnetic field (0,B_y,0) is centered in the middle of the dimuon magnet. No stray field is included. Inside the L3 volume a pure solenoidal field is set to 0.2 T.

- The muon stations are represented as aluminum sheets with a thickness of 2 % of radiation length per plane. The spatial measurement errors are introduced as gaussian smearing of the recorded hit positions from GEANT. A fixed spatial resolution of $5/\sqrt{12}$ mm is kept in the non-bending direction. The efficiency of the position detection is set to 95 % per plane. Double hit effects are neglected.

- For the particle production, the physics event generators described in Ref. [5] are included. In the case of the Φ production, the rapidity distribution is simply the one of the heavy vector mesons. A p_T distribution has been estimated using several dependances for the low and high p_T part of the Φ spectrum.

2 Acceptance

The purpose of the muon arm is to detect muon pairs in the mass range 1 - 10 GeV/c originating either from vector meson decays or from semimuonic decay of open charm and beauty which are used as normalisation. For the acceptance calculations, only the vector mesons have been used. The resonances are emitted in the apparatus and the correlated unlike sign muons are detected if they cross all the tracking stations and the trigger layers. A muon energy threshold around 4 GeV is observed due to the energy loss in the front absorber and in the iron wall of the trigger. In principle, an increase of the acceptance would be obtained by including muons stopping in the trigger wall. However, from the tracking point of view, the corrections of the multiple scattering and of the energy loss fluctuations will not be precise enough to preserve the requested mass resolution for these events.

2.1 Rapidity and Transverse Momentum Patterns

The geometrical acceptances, assuming uniform distributions in rapidity y and transverse momentum p_T, for the Φ, J/Ψ and Υ are shown in figure 2. For the two heavier vector mesons, 50 % of the maximum acceptance is reached between y = 2.8 and y = 3.6, whatever the p_T of the resonance is. In the case of the Φ, a pronounced decrease of detection is observed below p_T = 2.0 GeV/c at low rapidity due to the 4 GeV muon energy thresholds introduced both by the hadron and trigger absorbers. However, a decrease of the p_T cutoff can be observed at forward rapidity due to the Lorentz boost which entitle to extract physics even at low p_T.

Rapidity and transverse momentum dependences of the acceptance, for the vector mesons Φ, J/Ψ and Υ using physical distributions are displayed in figure 3. Without including the p_T thresholds at the trigger level, the acceptance of the J/Ψ and the Υ

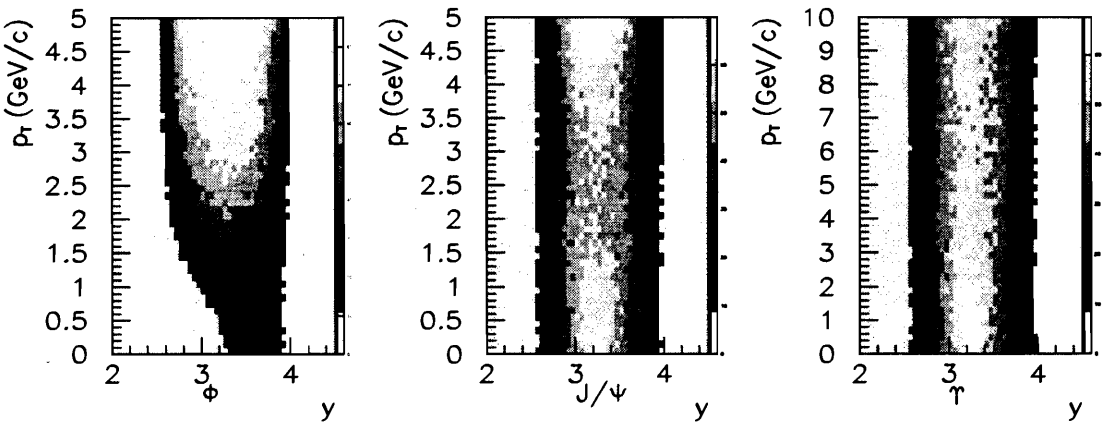

Figure 2: *Geometrical acceptance in rapidity y versus tranverse momentum p_T for the Φ, J/Ψ and Υ.*

looks bell-shaped in rapidity with a maximum up to 60 % at the mean rapidity y = 3.3. The 2.3 GeV/c p_T trigger cut on the individual muons doesn't change the rapidity pattern of the Υ's. As expected, a little decrease down to 45 % is observed for the J/Ψ's when introducing the 1 GeV/c trigger cut. In the p_T space, a flat pattern is observed even below p_T = 1.0 GeV/c for the heaviest meson. The 2.3 GeV/c p_T trigger cut leads to a loss of 20 % of the statistics in the high p_T region. For the J/Ψ, the reduction of the p_T acceptance issues from the muon momentum threshold introduced by the absorbers leads to a slightly unconstant behaviour. This tendance is amplified when introducing the 1 GeV/c trigger threshold. However, a quite good detection efficiency is still reached. A worst situation is observed for the $\Phi's$ leading to a quite low detection efficiency at low p_T due to the strong decrease of the p_T distribution of this resonance. For this state, the acceptance is only favorable at large p_T.

2.2 Summary of the Acceptance

The relative acceptances of the resonances, in the rapidity domain $2.5 < y < 4$ are summarized in the table 1. Absolute acceptances of these onia integrated over the total rapidity distribution are given as indications. Due to the transverse mass cutoff resulting from the energy threshold of the spectrometer, the integrated acceptance decreases rapidly with decreasing mass of the vector mesons.

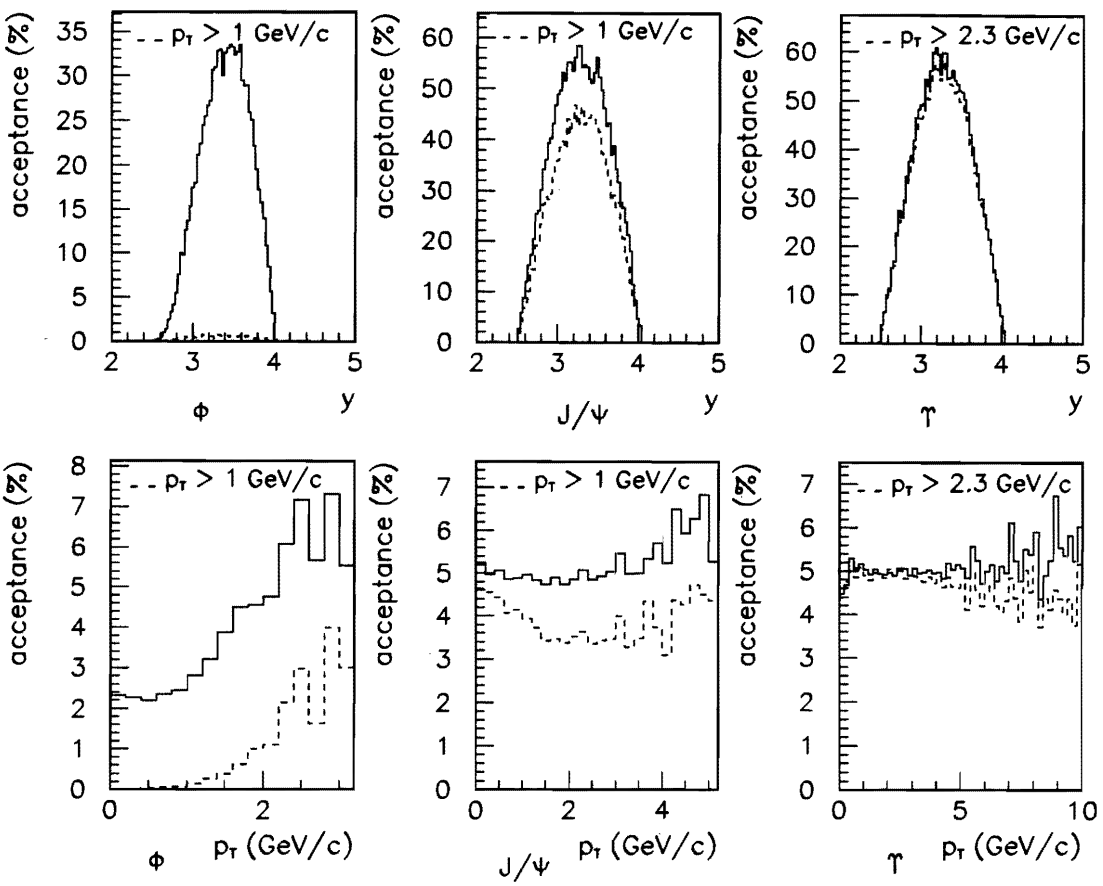

Figure 3: *Rapidity and transverse momentum dependence of the relative acceptance for the Φ, J/Ψ and ϒ. Results of the trigger cuts are in dotted lines.*

3 Track Finding

The track finding has been investigated with two major goals. On one hand, one has to save the maximum of detection of ϒ 's inside the enormous flux of mesons expected in the Pb-Pb collisions at LHC. On the other hand, the requiered mass resolution must remain below 100 MeV for these resonances. This leads to a compromise between track finding efficiency and momentum resolution which depend of scattering effects due to manyfold detection planes. The tracking method has been adapted to numerous different set-up configurations and physical scenario like the distance between the planes or the spatial resolutions of the tracking stations, as well as the particle densities. This section summarizes the results of these studies.

A detailed description of the track finding method has already been given in the LOI [3]. From the algorithms point of view, no fundamental change has been introduced.

	Φ	J/Ψ	Υ
Relative Acceptance (%)	17.87	36.86	37.15
Absolute Acceptance (%)	2.42	4.97	5.03
	Φ ($p_{T\mu}$ >1 GeV/c)	J/Ψ ($p_{T\mu}$ >1 GeV/c)	Υ ($p_{T\mu}$ >2.3 GeV/c)
Relative Acceptance (%)	0.57	29.85	35.66
Absolute Acceptance (%)	0.08	4.02	4.83

Table 1: *Summary of the relative and absolute acceptance of the muon spectrometer for the Φ, J/Ψ and Υ without and with the level 1 trigger thresholds.*

The track finding algorithm starts from the last muon stations. Inside the two planes of the downstream chambers, the hits are momentum ordered according to the approximated bending angle. Only muons of momenta greater than 2+3 GeV/c are kept. A straight line extrapolation is done to find the corresponding hits in the nearest downstream station, matching at least the position in one of the two planes of this station. Whenever this step is successful we try to backtrace the track upstream of the forward magnet with the help of the track fit, assuming that it trains on the interaction point and match with the hits of the three first muon stations. The track is considered to be found when the number of associated hits detected in the layers satisfies the global majorities of 3/4 for the upstream planes with 3/4 for the downstream planes and 1/2 for the in-magnet station. This procedure is continued until the completion of the candidat hits.

For central Pb–Pb collisions, charged multiplicities as high as $(dN/dy)_{y=0} = 8000$ are foreseen [10]. In order to simulate the collision products, the events were generated for the worst-case situation of central Pb–Pb collisions with a primary multiplicity of $(dN/dy)_{y=0} = 8000$ charged (π, K), plus $(dN/dy)_{y=0} = 4000$ neutral mesons (π^o, K^o) in the rapidity range $2 \leq y \leq 7$. In spite of the front hadron absorber, around 500 hits per plane were usualy found in the tracking chambers of the dimuon spectrometer during the simulations.

3.1 Tracking Station Requirements

Two chamber parameters play an important role for the pattern recognition, the double-plane spacing and the spatial resolution of the tracking stations. Because, inside the tracking station, the particle direction is defined by the position of the hit and the double-plane distance, both are linked for the track finding.

A first investigation concerning the double-plane distance of the downstream stations has been done in order to optimize the tracking efficiency. This spacing is of major importance because it defines the initial particle road at the begining of the track finding. The results are shown in figure 4 which displays the dependence of the track finding efficiency versus the double-plane distance. Good working conditions are achieved from the first

6 cm which exhibit a tracking efficiency still greater than 90 % with a negligeable ghost track rate below 1.6 % for the Υ. As expected, the large double-plane distances are more efficient at the begining of the track finding in spite that the higher impact combinatoric lies to a more time consuming procedure in order to connect the hits between the two planes. With 20 cm, the efficiency reaches 91.9 % when a decrease of the ghost track percentage is observed down to 0.2 % . From technical requirements at the level of tracking chambers, avantages have been found in the use of spacing below 10 cm. However, an increase of this distance can be envisaged depending of the final chamber choice.

One of the other tricky parameters of the track finding is the chamber resolution [11]. For the dipole field $(0,B_y,0)$, the spatial resolution σ_x in the bending plane plays an important role. Inspection of the tracking results has shown that the precision of the initial road in the two downstream stations was more dominated by the spatial resolution than by scattering inside the trackers. Estimation of the track finding efficiency versus σ_x has been done in order to derive the best compromise between performances and technical feasabilities of the tracking chambers. Figure 5 exhibits the σ_x dependence of the track finding efficiency. A satisfactory working point is obtained up to $\sigma_x = 100\mu m$.

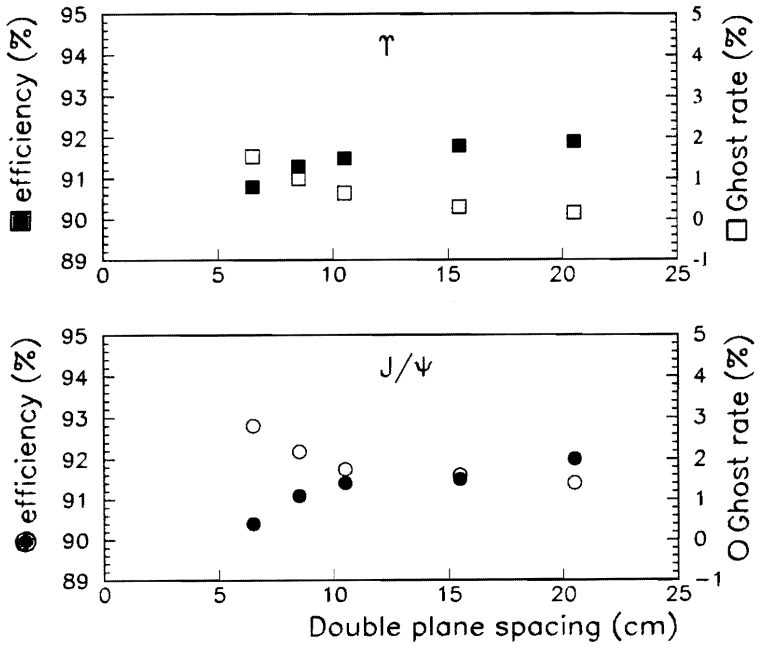

Figure 4: *Efficiency and ghost rate of the track finding for J/Ψ 's and Υ 's versus the double-plane distance of the two last stations for B.l = 3 T.m , σ_x = 100 μm.*

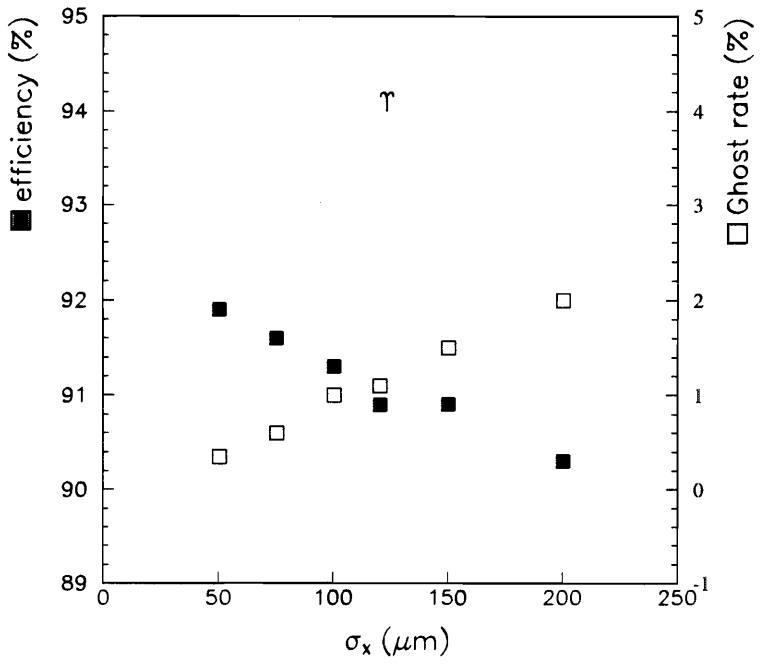

Figure 5: *Track finding efficiency and ghost rate versus the chamber resolution σ_x in the bending plane for Υ's with B.l = 3 T.m and 8 cm of double-plane distance.*

3.2 Robustness towards the Particle Density

Charged particle multiplicities and transverse momentum distributions foreseen for the LHC energies are still subject to large uncertainties. Other sources of uncertainty can arise directly from particle leakage due to the front absorber and the beam shielding. At the stage of GEANT, such effects are difficult to simulate. In this context it is significant to establish at which level of particle density the tracking may deteriorate. Efficiency of the pattern recognition for different particle multiplicities has been calculated. The general behaviour is shown in figure 6. A moderate decrease of the tracking efficiency is observed with the increase of the multiplicity. For 3 pile-up events, an efficiency over 87 % is still reached, which gives a very satisfactory safety marging. In spite of a factor 3 of increase, the ghost track rates stay acceptable around 2.6 % in this case. The mean number of reconstructed tracks per central Pb–Pb collisions for $(dN/dy)_{y=0} = 8000$ is 18.5 $\pm$2. As expected, this value is linearly correlated to the initial particle multiplicity.

3.3 Track Finding Conclusion

Good working conditions are obtained with B.l = 3 T.m and σ_y =1.4 mm for the set of following parameters:

- σ_x=100 μm

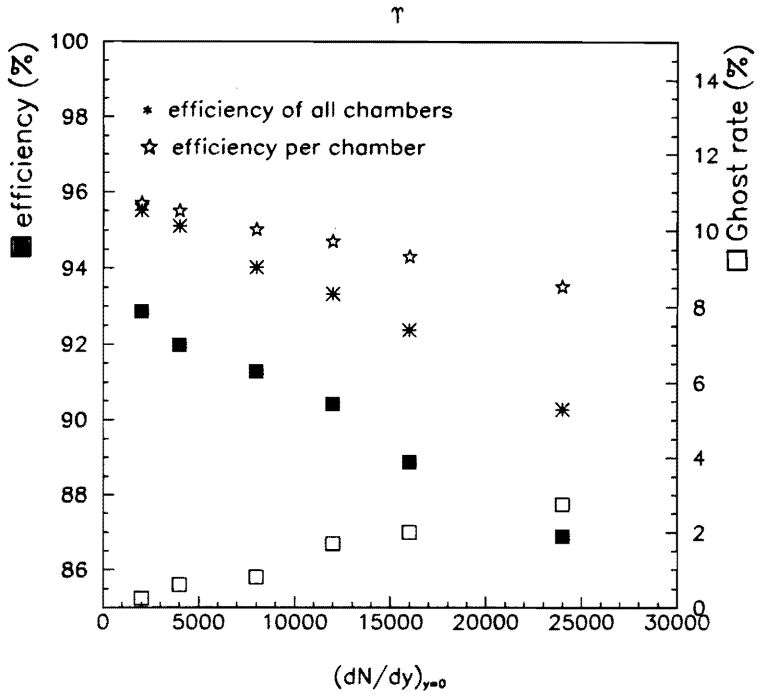

Figure 6: *Efficiency of the track finding for the* Υ *versus the particle density* $(dN/dy)_{y=0}$ *for* $B.l = 3\ T.m$, $\sigma_x = 100\ \mu m$ *and a plane spacing of 8 cm.*

- double plane distance of 8 cm
- expected particle multiplicity of $(dN/dy)_{y=0} = 8000$

In this case, an integral efficiency of 91.3 % and 91.1 % for the J/Ψ and the Υ reconstruction is obtained. The single track efficiency reached 95.5 % in which 3 % of inefficiency is due to the chamber itself (5 % inefficiency per plane) and 1.5 % of the track losses are due to confusion in the reconstruction algorithm.

In order to preserve the dimuon arm in operation in the case of the failures of one tracking station, simulations have been made with the nominal parameters given above but without the tracking station inside the muon magnet. Only the two downstream and upstream stations were used which constitutes from the track finding point of view the worst situation. Compared to the results with the full apparatus, a deficit of 3 % is observed in the tracking efficiency in which 2.6 % are directly issued from reconstruction error due to the absence of the magnet tracking chamber. The ghost track rate grows to 3 %.

4 Mass Resolution

The most important two-track parameter is the invariant mass resolution which should be as high as possible in order to provide a clear separation in the Υ familly. In order to reach the requiered mass resolution below 100 MeV, care must be taken especially from "in-acceptance" absorber material and chamber resolutions as well as from the integral field value. Results of the optimisation of these parameters are under the scope of this section.

Two main contributions drive the mass resolution of the spectrometer. At the level of the tracking chambers, classical sources of deteriorations like position resolution and alignment error added to multiple scattering affect the momentum resolution. In the given case of our set-up, another strong contribution comes from the energy loss fluctuation and the multiple scattering of muons in the hadron absorber. Corrections of these effects were performed inside a fast "mass finding program" in the following way:

- In a first step, the muon momentum is derivated without tacking into account the absorber effects. All hits associated to an identified track are fitted with no vertex constraints (i.e. the measured tracks after the hadron absorber are supposed uncorrelated with the vertex point). The track fit is a chisquare minimization using the MINUIT package with the five following parameters: the particle momentum p_{xz} in the bending plane, the two angles λ and ϕ which define the particle direction, and the two vertex coordinates x_V, y_V at $z = 0$. Correlations between the measurements in all the tracking stations due to multiple scattering effects are estimated with a covariance matrix. The matrix is calculated taking into account the spatial resolutions in each direction and the cumulated radiation length of the crossed medium [12]. At the end of this stage, the momentum parameters of the track at the exit of the front absorber are derived.

- During the second step, the optimisation of the emission angle of the particles at the vertex is inquired. This estimation plays a major role in the case of the detection through an absorber with small opening angles between the two muons. In this goal, both a Branson algorithm [13] and a mean energy loss correction are applied at the absorber level. Tracks are then enforced to join the vertex. At the end of this procedure, the final parameters of the particle at the emission vertex are derived.

The mass resolution at the resonance is calculated using a Gaussian fit in the (-1.5 σ, +2.5 σ) limits around the maximum of the mass distribution of the resonnance. Due to the assymetric nature of the Landau fluctuations in energy loss, the reconstructed mass distribution of the resonance exhibits a tail towards the low masses. However, no more than 10 % of the resonance events populated the low mass tail below the -1.5 σ limit with the Gaussian fit.

4.1 In-Acceptance Material Requirements

Out of punchthrough considerations, the main purpose of the absorber medium is to minimize all the sources of multiple scattering. For muons, coulomb scatterings from nuclei largely dominate. The main tunning point of the absorber optimisation lies entirely in the balance between the radiation length and interaction length of the medium. Larger must be the radiation length for a fixed interaction length. Up to this time, various absorber compositions have run in several experiments: Be [15] [16], C [6], Al [14] or Fe cores. With the 12° ALICE absorber, it is mandatory to find the best compromise between financial cost and mass resolution constraints. In order to extract the proper effect of the absorber material on the dimuon mass resolution, calculations using different media have been pursued. For these simulations, the geometrical configuration of the LOI absorber whith the same W setting-up stays unchanged. Only the absorber core was changed. Results of this systematic study are shown on figure 7 which exhibits the results of the mass resolution versus the absorber composition for a fixed 9 λ_I interaction length.

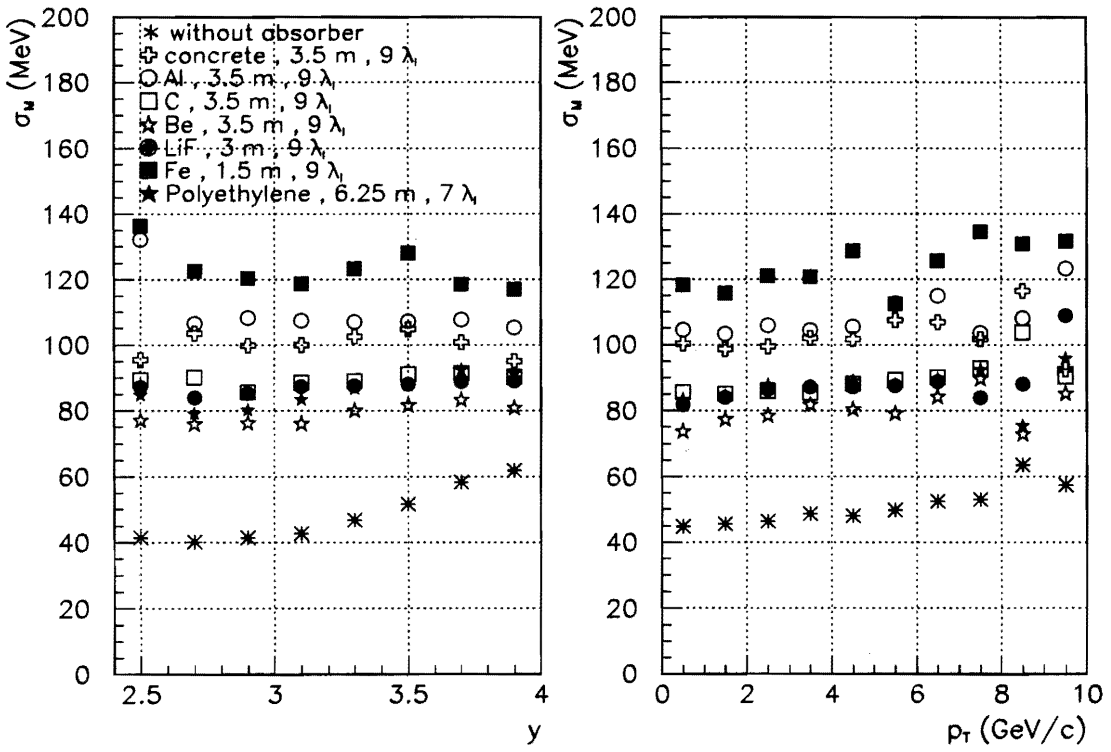

Figure 7: *Influence of the absorber material on the* Υ *mass resolution versus rapidity y and transverse momentum* p_T *for B.l = 3 T.m with* σ_x *= 100* μm*. Also indicated, the intrinsic mass resolution of the spectrometer without the front absorber.*

Comparisons with the no-absorber curves indicate at large angles that the resolution is dominated by straggling and multiple scattering in the absorber. Two classes of material can be distinguished. The first one corresponds to very low Z media: Be, C, polyethylene (monomer) and concrete which give equivalent performances. The second group, made of metals shows a worst behaviour which appears to be uncompatible with the requiered mass resolution. Best compromise was found when using a Carbon core for the absorber. At a lower cost, another possibility could lie in the use of a Carbon+concrete mixing in which the concrete ring is added at the end of the absorber. At the moment, this sandwich option is under study [7].

4.2 Tracking Station Requirements

Whereas, at low rapidities, the spectrometer resolution is dominated by multiple scatterings and energy loss fluctuations in the absorber, at high rapidities, the dominant contribution comes directly from spatial measurements of the tracking chambers. Two kind of actions have been pursued in order to diminish this underlined effect at high momenta.

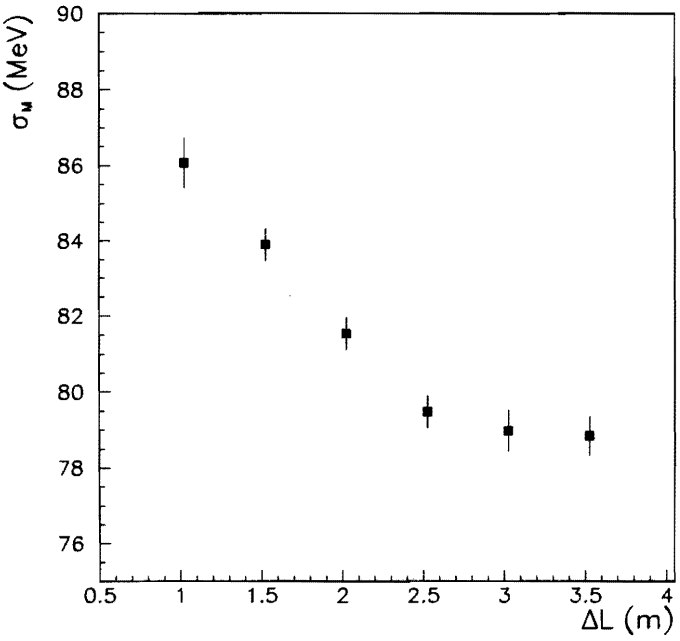

Figure 8: *Influence of the distance ΔL between the two last stations on the Υ mass resolution using a Carbon absorber with B.l = 3 T.m, σ_x = 100 μm.*

One of the ways lies in the tuning of the level arm between the two downstream stations (position of the two upstream stations are fixed due to constraints on the absorber

geometry). Figure 8 shows the effect of the distance between the two last tracking stations on the Υ mass resolution. The mass resolution of Υ improves with the increasing distance, until the contribution from multiple scattering due to the tracking stations themselves becomes the main source of uncertainty on the position measurements. This point is reached for a level arm of $\Delta L = 3$ m. However, due to track finding requirements in the task of matching tracks from the two stations, a suitable option is still obtained for $\Delta L = 2$ m when using a spatial resolution in the bending plane of $\sigma_x = 100$ μm .

Jointly, effects of excursions of the spatial resolution σ_x in the bending plane can also be investigated. Less steeply improvements are obtained with the decrease of σ_x as shown in Figure 9. The gain in the mass resolution is less than 10 MeV when changing σ_x from 100 μm to 50 μm. From a technological point of view, improvement of the spatial resolution will be difficult. A spatial resolution of 100 μm has been considered as satisfactory.

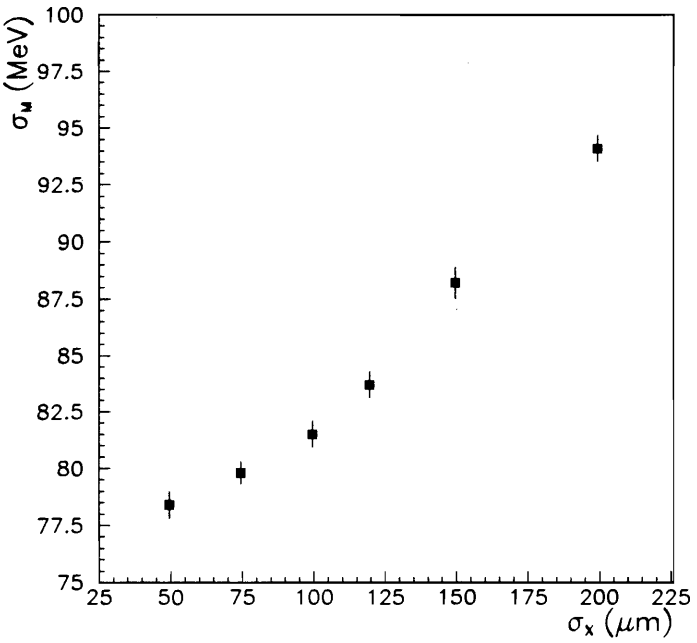

Figure 9: *Mass resolution for the Υ as a function of the resolution σ_x of the tracking stations in the bending plane. (B.l = 3 T.m, $\Delta L = 2$ m) .*

4.3 Integral Magnetic Field Dependence

The integral field of the dipolar magnet is one of the main parameter of the dimuon spectrometer. It governs its capability to analyze high momentum muons coming from Υ decays and influence to a lower level the track finding efficiency as well as the background rejection of the trigger. In this section we are dealing only with the mass resolution which

is shown to have a sharp dependence with the field integral. Figure 10 displays the behaviour of Υ mass resolution versus different field integral values. A conservative choice of B.l = 3 Tm has been made for which the mass resolution is well below 100 MeV. Even with a decrease of the magnetic field integral down to B.l = 2 Tm, the requested mass resolution will be secured.

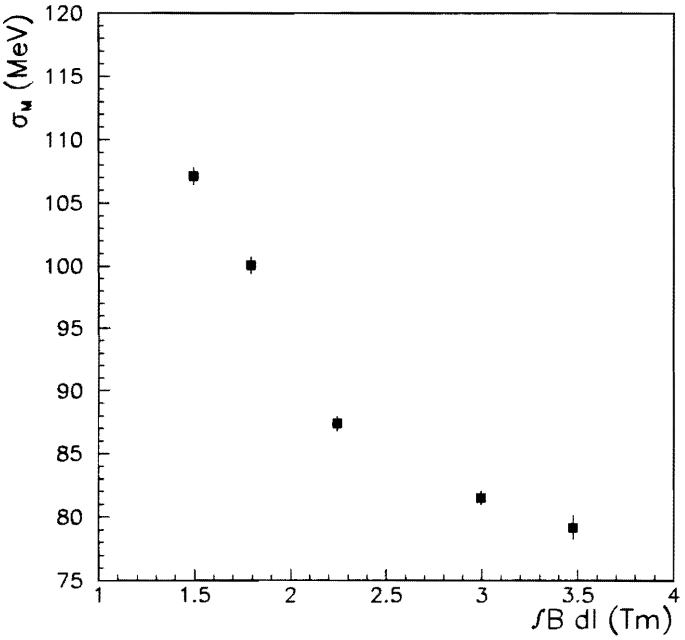

Figure 10: *Effect of the integral magnetic field for the Υ mass resolution with the tracking parameters: σ_x = 100 μm and ΔL = 2 m.*

4.4 Summary of the Mass Resolution Performances

The dimuon mass resolution has been calculated including the momentum resolution, multiple scattering in the absorber and imposing the interaction vertex as a constraint. Tunning of the tracking parameters lead to satisfactory performances using:

- a 9 λ_I carbon absorber,
- an integral magnetic field with B.l = 3 Tm,
- spatial resolutions σ_x = 100 μm and σ_y =1.4 mm.

Figure 11 displays the dependence of the mass resolution on p_T and rapidity for both J/Ψ and Υ with the set of parameters given above. The mass resolution in the Υ mass region is in all accessible kinematical region well below 100 MeV, which is sufficient for the clear

separation of Υ and Υ' signals. For J/Ψ, we obtain even a little bit better results around 66 MeV. (In the Φ region, a mass resolution below 55 MeV has been found).

In order to preserve fair running conditions of the dimuon arm in the case of the failures of one tracking station, simulations have been made with no tracking station inside the muon magnet. Only the two downstream and upstream stations have been used. Compared to the results with full apparatus, never more than 10 MeV of shading off in the Υ mass resolution is observed.

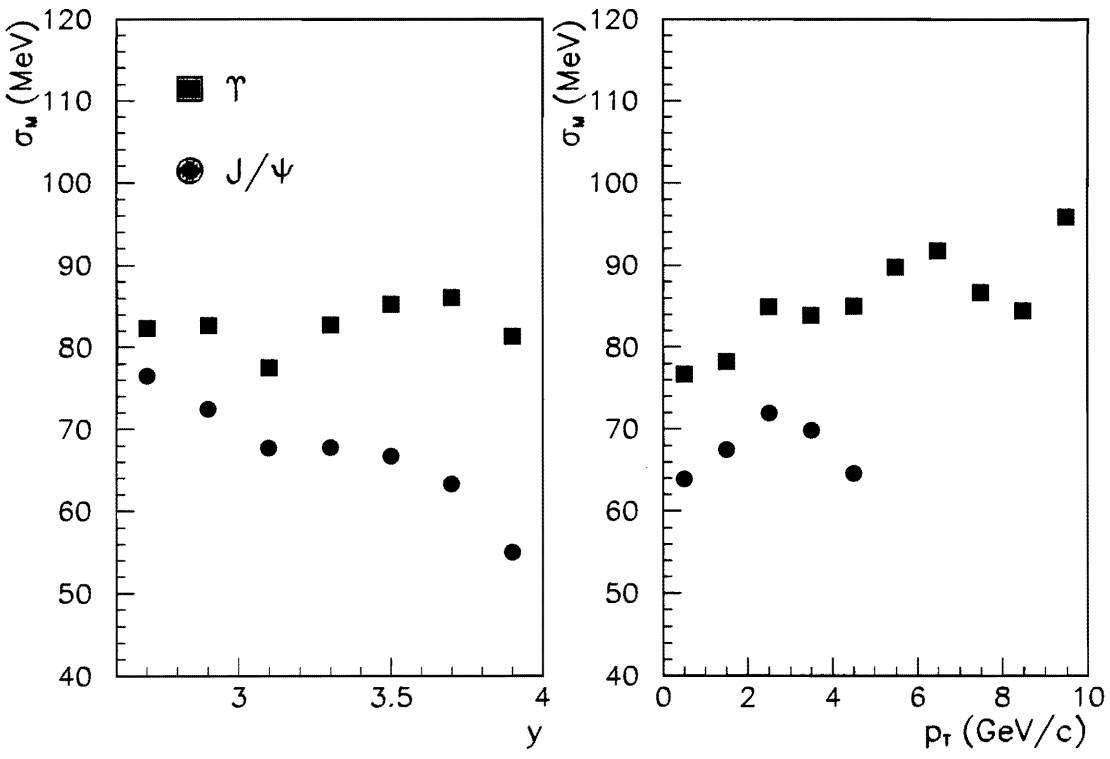

Figure 11: *Summary of the mass resolution performances versus rapidity y and transverse momentum p_T for the J/Ψ and the Υ.*

References

[1] Z. V. Borisovskaya et al. (JINR Dubna), ALICE internal note 95-08.

[2] RRC Kurchatov inst., ALICE internal note 95-10.

[3] ALICE Collaboration, Debye Screening in Heavy-Ion Collisions with the ALICE Detector, CERN/LHCC/95-24.

[4] ALICE Technical Proposal, CERN/LHCC/95-71.

[5] K. Eggert and A. Morsch, AT Group Report 95-01(DI) and ALICE Internal Note ALICE 95-05.

[6] L. Anderson et al. Nucl. Instr. Meth. 223 (1984) 26.

[7] A. Morsch, Private Communication, Alice-Dimuon Meeting (1996).

[8] ATLAS Technical Proposal, CERN/LHCC/94-43.

[9] D. Jouan and A. Lafoux, Private communication (1995).

[10] H. Satz, Phys. A544 (1992) 371.

[11] R. K. Bock, H. Grote. D. Notz and M. Regler, Data Analysis Techniques for High-Energy Physics Experiments, Cambridge University Press (1990).

[12] W. Blum and L. Rolandi, Particle Detection with Drift Chambers, Springer-Verlag (1994).

[13] J. G. Branson et al., Phys. Rev. Lett. 38 (1977) 1331.

[14] M. Masera et al., QM95 Nucl. Phys. A590 (1995) 93c.

[15] C. Biino et al., Nucl. Instr. Meth. A243 (1986) 323.

[16] D. E. Jaffe et al., Phys. Rev. D40 (1989) 2777.

(This report is also published in the ALICE collaboration under the reference ALICE Note 96-32)